Google Scholar Crossref doi scopus

Impact factor 6.2

Geoscience Journal

ISSN:1000-8527

Indexing:

- Scopus
- Google Scholar
- DOI, Zenodo
- Open Access

www.geoscience.ac

Registered

A GENERAL FORM OF EXERGY CHANGE CAPTURING THERMAL AND CALORIC IMPERFECTIONS IN OPEN AND CLOSED SYSTEMS

M.Salhi[1, 3,*], B. Ali Benyahia[2, 3], S. Bensedira[1, 3], N. Bengherbia[3]

[1]LTSM Laboratory
[2]Structure Laboratory
[3]Mechanical Engineering Department, Faculty of Technology
University of Blida 1, P.O. Box 270 Blida 09000 Algeria.

Abstract: A new, broadly applicable exergy formulation is presented, built directly on real gas thermodynamics theory and explicitly incorporating both thermal and caloric imperfections. It overcomes the inherent restrictions of classical perfect gas models and offers a single framework suitable for describing energy exchanges in realistic real gas conditions. The robustness of the formulation is examined numerically over several thermodynamic regimes. For open systems, it is tested and investigated on a supersonic isentropic nozzle, whereas for closed systems, it is applied to an isochoric air tank process and to an isobaric process represented by a piston cylinder setup. Comparisons are made between real gas and both the high temperature HT and the conventional perfect gas PG models show that the new expression predicts real gas behavior and energetics potential with higher accuracy. Results from previous models can differ from the current model by up to 30%.The results demonstrate that it can resolve the combined influence of the thermal and caloric imperfections and temperature-pressure effects on energy transfer and conversion. Together, these findings advance real gas exergy theory and support more realistic, predictive and efficient modeling of modern thermodynamic and propulsion systems.

Keywords: ***Exergy, Open and closed Systems, High temperatures-high pressures, Real gas model, Thermal and caloric imperfections.***

1. INTRODUCTION

Energy is a central concept in thermodynamics, expressing how much ability a system has to do work or transfer heat during a given change of state [1]. The first law guarantees that this energy is conserved, but it says nothing about how useful that energy is or how much of it can realistically be turned into work [2]. This gap is addressed by the notion of exergy, which characterizes not only the amount of energy present, but also how efficiently it can be converted into useful work under actual environmental and operating conditions [3]. Foundational contributions have helped establish exergy as a key method for analyzing and optimizing energy systems [4]. In most of these studies, the working fluid is modeled as a perfect gas, meaning its molecules are treated as non-interacting point masses, which allows thermodynamic relations to be expressed with relatively simple mathematical expressions [5].

Exergy analysis is valuable because it can identify and measure irreversibilities. These irreversibilities are inherent losses in real processes that reduce energy's usefulness [6, 7]. Unlike energy, which is always conserved, exergy is destroyed when entropy is created [8]. Therefore, exergy analysis provides a more accurate way to assess process efficiency and sustainability [9]. However, despite its theoretical soundness and wide use in many areas from power generation to fuel cell studiesmost traditional exergy methods and their later developments still rely heavily on the perfect gas model. This reliance limits their accuracy in extreme or non-ideal situations [10].

The prevalence of this constraint is evident in recent scholarly work. For example, investigations into sophisticated energy–exergy analyses of contemporary systems offer novel insights into exergetic breakdown and enhancement [11–14]. However, these studies' methodological approaches are fundamentally based on ideal gas assumptions. This limitation is especially significant when simulating high temperature, high pressure systems, where departures

from idealized behavior are substantial. Consequently, this reliance restricts the practical application of traditional exergy theory to actual conditions, which are defined by molecular interactions, temperature-dependent specific heats, and state-dependent thermodynamic characteristics.

To rectify these limitations, a number of core thermodynamic investigations have examined gas behavior at elevated temperatures, focusing on modifications that broaden the applicability of established models. Foundational works analyze the intricacies of high temperature phenomena, providing correction factors for thermodynamic properties including enthalpy, entropy, and specific heats [15–17]. In addition to this theoretical foundation, a multitude of analytical and numerical studies have formulated novel expressions for supersonic and hypersonic flow parameters [18–22], revising the Prandtl–Meyer function [23] and nozzle design principles to account for non-ideal gas behaviors [24]. These contributions highlight the necessity of moving beyond perfect gas assumptions when characterizing thermodynamic systems functioning at high temperatures.

Even in some of the earliest work, such as that of Donaldson [25], researchers already understood that neither the perfect gas model nor the first high temperature corrections were sufficient to describe how real gases actually behave at the molecular level. More recently, authors in reference [26] showed that vibrational energy and intermolecular forces can strongly affect calorimetric and thermoelastic coefficients, creating clear gaps between what experiments measure and what simplified theories predict. Taken together, these findings make it clear that both ideal and semi-ideal models fall short when trying to represent real gases, especially under extreme thermal and calorific conditions.

In response to these constraints, recent investigations have integrated real gas theory, which simultaneously considers pressure, temperature, and vibrational influences, to refine established thermodynamic models. Many references have introduced sophisticated models for flow parameters [27–29], Prandtl–Meyer functions [30–32], and nozzle performance, specifically incorporating thermal and calorific deviations [33, 34]. Furthermore, these studies have broadened the application of real gas corrections to fundamental thermodynamic potentials, encompassing internal energy ΔU and the work W [35], the enthalpy ΔH [36], the entropy ΔS [37], and Gibbs and Helmholtz free energies ΔG and ΔF [38]. Consequently, their combined results have demonstrated that neglecting temperature–pressure-dependent imperfections results in significant estimation inaccuracies when assessing both energy transformations and exergy destruction.

In light of this expanding research, the present investigation endeavors to formulate and numerically analyze a novel, generalized exergy model, grounded in the principles of real gas behavior. This model's objective is to consolidate energy and exergy concepts by incorporating the authentic characteristics of gases encompassing thermal, calorific, and pressure influences within the exergy paradigm. Unlike earlier models constrained by idealized or simplified assumptions, the proposed formulation seeks to improve predictive precision across a broad spectrum of thermodynamic scenarios, spanning from low-enthalpy environmental systems to high-enthalpy aerospace propulsion flows.

The primary objective of the paper was to numerically examine a novel model of exergy change. The development of a realistic, generalized exergy formulation constitutes a substantial scientific achievement, effectively connecting theoretical thermodynamics with its practical applications. This research enhances the precision of exergy analysis by integrating real gas behavior and eliminating the limitations inherent in the perfect gas model. Furthermore, it establishes a universal thermodynamic framework that can characterize energy quality across all physical conditions. To accomplish this, the thermodynamic equations were formulated employing Berthelot's equation of state, which offers estimations of intermolecular force impacts, in contrast to the Van der Waals state equation. A method to augment the accuracy and efficacy of current models for calculating exergy alterations involves considering the effects of temperature, pressure, and well, alongside thermal and caloric imperfections. It is expected that the Planck expression, in terms of CP and CV, could potentially characterize caloric imperfections. Furthermore, it establishes a universal thermodynamic framework that can characterize energy quality across all physical conditions. This advancement has far-reaching consequences for high-efficiency energy conversion technologies, aerospace propulsion systems, and sustainable engineering practices, where a comprehensive understanding of energy conversion's true potential is essential for both innovation and environmental stewardship.

2. Mathematical formulations

A- Exergy:

The exergy, which measures energy quality rather than just quantity and is zero at the dead state when the system and environment are in perfect equilibrium, is the maximum useful work that a system can produce as it reversibly enters equilibrium with a particular environment (dead state). Depending on the nature of the system, it can be defined as follows [3]:

$$Ex = (U - U_0) + P_0 (v - v_0) - T_0 (S - S_0) + KE + PE \tag{1}$$

Where KE and PE represents the kinetic and potential energies, respectively, and (0) indicates environmental properties (dead state).

Equation (1) is specific to closed systems, when heat and work can be exchanged, but mass can not exceed its border; hence, the specific exergy variation for a closed system between two states (1) and (2) is given by[4]:

$$\Delta ex_{CS} = (u_2 - u_1) + P_0 (v_2 - v_1) - T_0 (s_2 - s_1) + \left(V_2^2 - V_1^2\right)/2 + g (Z_2 - Z_1) \tag{2}$$

Otherwise, an open system allows mass, heat, and work to cross its boundary, so exergy is associated with mass flow as well, the specific exergy of a flowing stream is often defined by[4]:

$$ex_{OS} = (h - h_0) - T_0 (s - s_0) + KE + PE \tag{3}$$

The specific exergy variation for an open system between state (1) and state (2) is given by[6]:

$$\Delta ex_{OS} = (h_2 - h_1) - T_0 (s_2 - s_1) + \left(V_2^2 - V_1^2\right)/2 + g (Z_2 - Z_1) \tag{4}$$

It should be mentioned that the exergy and free energy, or free enthalpy, have a significant relationship, as fellows [2]:

$$\Delta ex_{CS} = \Delta F - T_0 \Delta S \tag{5}$$

and

$$\Delta ex_{OS} = \Delta G - T_0 \Delta S \tag{6}$$

In thermodynamics, the general exergy balance for closed system is [5]:

$$X_{in} - X_{out} - X_{destroyed} = X_{system} \tag{7}$$

Where, the exergy destroyed is defined by[1]:

$$X_{destroyed} = T_0 S_{generation} \tag{8}$$

The entropy generation is not only the entropy system but is the sum of entropy system and entropy surrounding[7].

$$S_{gen} = \Delta S_{System} + \Delta S_{Surrounding} \tag{9}$$

So that [1]:

$$\Delta S_{Surrounding} = Q/T_0 \tag{10}$$

In a steady state, an open system's general energy rate balance is [9]:

$$\frac{d\,EX}{d\,t} = 0 \Rightarrow \sum \dot{m}\, ex_{in} - \sum \dot{m}\, ex_{out} + \sum \dot{X}_Q - \dot{X}_W - \dot{X}_{destroyed} = 0 \tag{11}$$

Where: ex_{fin} and ex_{fout} are the specific flow exergy or terms accounts for the exergy per unit of mass entering at inlet and outlet, $\dot{X}_Q$ the exergy transfer accompanying heat transfer, $\dot{X}_W$ the rate of exergy transfer accompanying the work W and $\dot{X}_{destroyed}$ the rate of exergy destruction within the control volume[8].

$$0 = \sum_J \left(1 - \frac{T_0}{T_J}\right) \dot{Q}_J - \dot{X}_W + \sum \dot{m}\, ex_{fin} - \sum \dot{m}\, ex_{fout} - \dot{X}_{destroyed} \tag{12}$$

The specific flow exergy is given by[10]:

$$ex_f = (h - h_0) - T_0 (s - s_0) + V^2/2 + g \cdot z \tag{13}$$

The relationship between specific flow exergy ex_f and specific exergy ex is[12]:

$$ex_f = ex + v(p - p_0) \tag{14}$$

In supersonic nozzles, there is a single inlet and a single exit, denoted by 1 and 2, respectively, and no works inside the volume control $\dot{X}_W = 0$, the exergy rate balance reduces to[13]:

$$0 = \sum_J \left(1 - \frac{T_0}{T_J}\right) \dot{Q}_J + \dot{m}\left[\left(h_2 - h_1\right) - T_0\left(s_2 - s_1\right) + \left(V_2^2 - V_1^2\right)\Big/2 + g\left(Z_2 - Z_1\right)\right] - \dot{X}_{destroyed} \quad (15)$$

Otherwise, the exergy transfer accompanying work is the difference between the boundary work (total work) W_b and the work needed to push the environment (the surroundings work) and can be expressed by [11]:

$$\dot{X}_W = W_b - P_0 \Delta v = \int P\,dv - P_0 \Delta v \quad (16)$$

At high altitude, the environmental temperature and pressure can be computed as follows [15]:

$$T_0^Z = \left(-0.0066 \times Z\right) + T_0^{Z=0} \quad (17)$$

$$P_0^Z = P_0^{Z=0} \times e^{\left(\frac{\mathfrak{M} \times g \times z}{r \times T_0^Z}\right)} \quad (18)$$

B- Real gas model:

Real gas theory provides more accurate exergy and exergy-destruction values at high pressures and temperatures by better capturing variances from previous models. This promotes improved analysis, design and optimization by increasing the accuracy of efficiency and loss predictions in systems.

The Berthelot state equation in real gas theory is provided by [33]:

$$P(T,v) = \frac{RT}{(v-b)} - \frac{a}{T v^2} \quad (19)$$

Or:

$$P(T,\rho) = \frac{\rho RT}{(1-\rho b)} - \frac{a\rho^2}{T} \quad (20)$$

The molecular size and intermolecular force coefficients for BSE are: $a = 3 P_c V_c^2 T_c$ and $b = \frac{V_c}{3}$ where Pc, Vc, and Tc indicate temperature, pressure, and volume, respectively.

Table 1. Air parameters

Critical parameter	air
Critical temperatureTc [K]	132.5
Critical pressure Pc [pas]	$37.7 * 10^6$
Critical volume Vc [m^3]	0.00322
Gas constant R [J/kg K]	287
Specific heats ratio GP γ	1.4
Constant of molecular vibrational energy θ [K]	3056
Specific heat capacity CP-GP [KJ/kg K]	1.004

The specific heats at constant pressure C_P and volume $C_V$is provided by [27, 29]:

$$C_v(T,\rho) = C_{vPG}\left\{1 + (\gamma_{PG} - 1)\left(\left(\frac{\theta}{T}\right)^2 \frac{z}{(1-z)^2} + \frac{2a\rho}{RT^2}\right)\right\} \quad (21)$$

$$C_p(T,\rho) = C_{P_{PG}}\left[1 + \left(\frac{\gamma_{PG} - 1}{\gamma_{PG}}\right)\left\{\left(\frac{\theta}{T}\right)^2 \frac{Z}{(1-Z)^2} + \frac{2a\rho}{RT^2}\left[1 + \frac{\left(\frac{2 - b\rho}{1 - b\rho} + \frac{a\rho}{2RT^2}\right)}{\frac{1}{(1-b\rho)^2} - \frac{2a\rho}{RT^2}}\right]\right\}\right] \quad (22)$$

We have; $z=e^{\left(\frac{\theta}{T}\right)}$, $z_0=e^{\left(\frac{\theta}{T_0}\right)}$

In thermodynamics, we can characterize or present each state function by two state variables, then: The enthalpy change for real gas model is given by [36]:

$$\Delta H=\int_{T_1}^{T_2} C_P(T,\rho)\big|_{\rho=\rho_2}\,dT+\int_{\rho_1}^{\rho_2} C_T(T,\rho)\big|_{T=T_2}\,d\rho \tag{23}$$

Where [28]:

$$C_T(T,\rho)=\left(\frac{3ab^2\rho^3-6ab\rho-RT^3b+3a}{2T\rho b-Tb^2\rho^2-T}\right) \tag{24}$$

The variation of U for real gases gives [35]:

$$\Delta U=\int_{T_1}^{T_2} C_V(T,\rho)\big|_{\rho=\rho_2}\,dT-\int_{\rho_1}^{\rho_2}\left(\frac{2\,a}{T}\right)\Big|_{T=T_2}\,d\rho \tag{25}$$

The work received during an isothermal process, isobaric process and for an adiabatic process are respectively given by [35]:

$$W_{T=Const}=RT_1\,ln\left(\frac{v_1-b}{v_2-b}\right)+\left[\frac{a\,(v_2-v_1)}{v_1v_2\,T_1}\right] \tag{26}$$

$$W_{P=Const}=-P\,(v_2-v_1) \tag{27}$$

$$W_{adia}=\frac{P_2v_2-P_1v_1}{\gamma(T,\rho)-1} \tag{28}$$

The specific heats ratio γ for the real gas is given by [26, 34]:

$$\gamma\,(T,\rho)=\frac{Cp\,(T,\rho)}{Cv\,(T,\rho)} \tag{29}$$

The change in entropy for real gas model can be obtained from [37]:

$$\Delta S(T,\rho)=R\int_{T_1}^{T_2}\left(\frac{C_V(T,\rho)}{RT}\right)dT+R\int_{\rho_1}^{\rho_2}\left(\frac{1}{\rho(\rho b-1)}-\frac{a}{RT^2}\right)d\rho \tag{30}$$

The change in Gibbs free energy is given by [38]:

$$\Delta G_{Sys}(T,\rho)=\int_{T_1}^{T_2} C_P(T,\rho)\big|_{\rho=\rho_2}\,dT+\int_{\rho_1}^{\rho_2} C_T(T,\rho)\big|_{T=T_2}\,d\rho-T.R.\left[\int_{T_1}^{T_2}\left(\frac{C_v(T,\rho)}{RT}\right)dT+\int_{\rho_1}^{\rho_2}\left(\frac{1}{\rho(\rho b-1)}-\frac{a}{RT^2}\right)d\rho\right] \tag{31}$$

Conversely, the change in Helmholtz free energy is [38]:

$$\Delta F_{Sys}(T,\rho)=\int_{T_1}^{T_2} C_V(T,\rho)\big|_{\rho=\rho_2}\,dT-\int_{\rho_1}^{\rho_2}\left(\frac{2\,a}{T}\right)\Big|_{T=T_2}\,d\rho-T.R.\left[\int_{T_1}^{T_2}\left(\frac{C_v(T,\rho)}{RT}\right)dT+\int_{\rho_1}^{\rho_2}\left(\frac{1}{\rho(\rho b-1)}-\frac{a}{RT^2}\right)d\rho\right] \tag{32}$$

The flow velocity for open systems is given by [30]:

$$V^2(T,\rho)=2\left\{C_{v_{PG}}(T_0-T)+R\theta\left(\frac{1}{(1-Z)}-\frac{1}{(1-Z_0)}\right)+4a\left(\frac{\rho}{T}-\frac{\rho_0}{T_0}\right)+\left(\frac{p_0}{\rho_0}-\frac{p}{\rho}\right)\right\} \tag{33}$$

The speed of sound of the gas flow is [32]:

$$C_S^2(T,\rho)=\frac{RT}{(1-b\rho)^2}-\frac{2a\rho}{T}+\frac{\rho^2T\left(\frac{a}{T^2}+\frac{R}{\rho(1-b\rho)}\right)^2}{C_{v_{PG}}\left[1+(\gamma_{PG}-1)\left\{\left(\frac{\theta}{T}\right)^2\frac{Z}{(1-Z)^2}+\frac{2a\rho}{RT^2}\right\}\right]} \tag{34}$$

$$M^2(T,\rho)=\frac{V^2(T,\rho)}{Cs^2(T,\rho)} \tag{35}$$

The energy equation for compressible isentropic flow is given by[14, 31]:

$$h_1+\frac{V_1^2}{2}=h_2+\frac{V_2^2}{2}\Rightarrow \Delta H+\left(\frac{V_2^2-V_1^2}{2}\right)=0 \tag{36}$$

SO, the integral form of energy equation became [36]:

$$\int_{T_1}^{T_2} C_P(T,\rho)\big|_{\rho=\rho_2}\,dT+\int_{\rho_1}^{\rho_2} C_T(T,\rho)\big|_{T=T_2}\,d\rho+\left(\frac{V_2^2-V_1^2}{2}\right)=0 \tag{37}$$

3. Validation of the exrgy variation

The numerical validation of the new exergy model based on real gases for open and closed systems have been carried out using several representative test cases. First, an isentropic flow through a supersonic MLN nozzle was studied to analyze the exergy behavior under large velocity and pressure variations along a compressible flow. Then, two equivalent closed systems were considered to complete the analysis: an isochoric process, modeled by an air tank, and an isobaric process, represented by a piston-cylinder system. All of these conFigureurations were simulated numerically using Fortran code within the PowerStation environment, which allowed verification of the consistency of the new exergy model with the laws of thermodynamics and available reference results for HT and GP models.

A. High temperature Model:

A high temperature model HT is a simplified physical or mathematical representation of a system that describes how it behaves at high temperatures where thermal effects are dominant. Based on the perfect gas theory (thermally perfect gas), but C_P and C_V change with temperature (calorically imperfect gas)[16, 25].

The change in enthalpy, internal energy, the entropy and the velocity for HT model are [17–22]:

$$\Delta H=\int_{T_1}^{T_2} C_P(T)\;dT \tag{38}$$

$$\Delta U=\int_{T_1}^{T_2} C_V(T)\;dT \tag{39}$$

$$\Delta S=\int_{T1}^{T2}\frac{C_V(T)}{T}\,dT+R\ln\frac{P_1}{P_2} \tag{40}$$

$$V=\sqrt{2H(T)} \tag{41}$$

Tables 2 and 3 provide the 9th and 10th polynomials of Cp and γ for air sequentially [24].

$$C_P(T)=\sum_{i=1}^{10} a_i\;T^{(i-1)} \tag{42}$$

$$\gamma(T)=\sum_{i=1}^{11} b_i\;T^{(i-1)} \tag{43}$$

Table 2. Polynomial Coefficients of C_P (T) [23].

i	ai

1	1001.1058
2	4.0661289 10-2
3	-6.3376997 10-4
4	2.7474759 10-6
5	-4.0338459 10-9
6	3.0697736 10-12
7	-1.3509355 10-15
8	3.472262 10-19
9	-4.8467531 10-23
10	2.8411878 10-27

Table 3. Polynomial Coefficients of γ(T) [23].

i	bi
1	1.4030049
2	-4.8380251 10-05
3	5.7713164 10-07
4	-2.4333247 10-09
5	4.1173757 10-12
6	-3.8217601 10-15
7	2.1579012 10-18
8	-7.6237753 10-22
9	1.6491564 10-25
10	-1.999789 10-29
11	1.0420059 10-33

The specific heat at volume constant C_V for HT model is [15, 19]:

$$C_V(T) = \frac{C_P(T)}{\gamma(T)} \tag{44}$$

The work received during an isothermal process, isobaric process and for an adiabatic process are respectively given by [1, 7]:

$$W_{T=Const} = n\,R\,T \ln\left(\frac{v_2}{v_1}\right) = n\,R\,T \ln\left(\frac{P_1}{P_2}\right) \tag{45}$$

$$W_{P=Const} = -P\left(v_2 - v_1\right) \tag{46}$$

$$W_{adia} = \frac{P_2 v_2 - P_1 v_1}{\gamma(T) - 1} \tag{47}$$

B. Perfect gas Model

Otherwise, A perfect gas model treats a gas as ideal, which means that molecules follow the ideal gas law PV=nRT, have negligible volume, and have no intermolecular interactions. This expression additionally points to constant specific heats Cp and Cv in many thermodynamics texts, meaning that internal energy and enthalpy are solely dependent on temperature. The relationships of this model are presented as follows [4, 9]:

$$C_V = \frac{r}{\gamma - 1} \tag{48}$$

$$C_P = \frac{\gamma \,.\, r}{\gamma - 1} \tag{49}$$

$$\Delta H = C_P\,\Delta T \tag{50}$$

$$\Delta U = C_V\,\Delta T \tag{51}$$

$$\Delta S = C_V \ln\left(\frac{T_2}{T_1}\right) + R \ln\frac{P_1}{P_2} \tag{52}$$

The work received during an isothermal process, isobaric process and for an adiabatic process are respectively given by [10, 11]:

$$W_{T=Const} = n\,R\,T\ln\left(\frac{v_2}{v_1}\right) = n\,R\,T\ln\left(\frac{P_1}{P_2}\right) \tag{53}$$

$$W_{P=Const} = -P\left(v_2 - v_1\right) \tag{54}$$

$$W_{adia} = \frac{P_2\,v_2 - P_1\,v_1}{\gamma - 1} \tag{55}$$

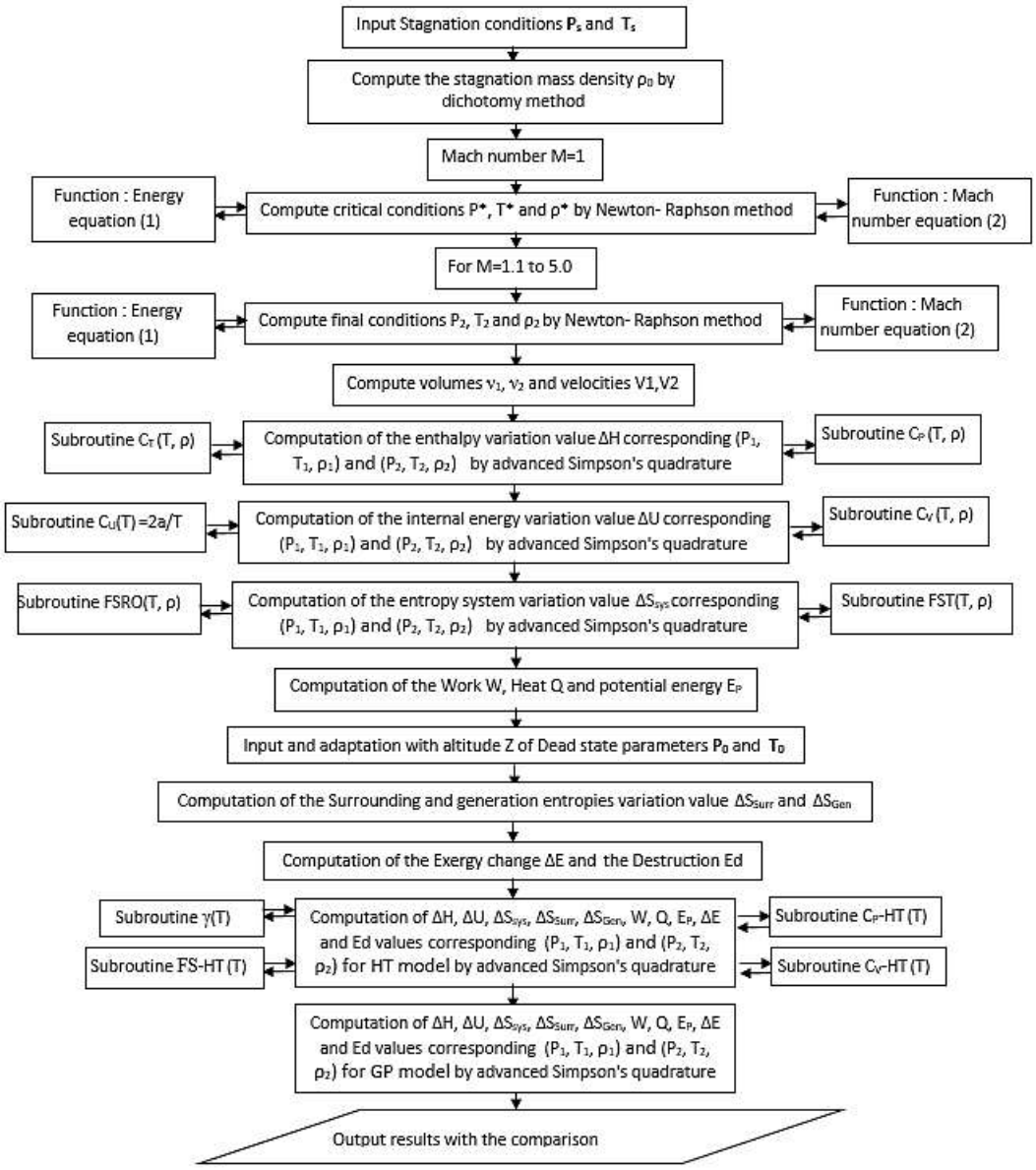

Figure 1. The basic steps of exergy change computation for isentropic and compressible fluid flow

. Numerical exergy analysis typically unfolds in a few computational steps that combine root finding with numerical integration of thermodynamic properties. For each of the two states initial (1) and final (2), the density is first computed by solving the equation of state with the bisection method[39, 40], where the solution is bracketed between two values that give opposite signs and the interval is gradually reduced until the target accuracy is met[41]. After the properties at each state are known, the required integrals of enthalpy, entropy, and internal energy are then evaluated numerically; often using Simpson's method with an adaptive step size to obtain the exergy [42, 43].This allows the step size to be adjusted according to the variation of the properties and limits the integration error. The case of the supersonic isentropic system is more complex[41],

because the initial and final conditions (pressure, temperature, density) are no longer directly accessible through simple integration[44, 45], but result from the simultaneous solution of a system of nonlinear equations coupling the Mach number, the energy equation, and the Berthelot equation for the real fluid. In this situation, the Newton-Raphson method is used to quickly obtain the solution to the system, by iteratively linearizing the equations around an initial estimate and updating the unknowns until convergence [43]. This allows for the consistent determination of all the thermodynamic input and output parameters for the final exergy calculation.The following diagram illustrates the basic steps of exergy change computation for isentropic and compressible fluid flow

4. Results and discussion

In this section, we proceed to the presentation of the various results obtained by an elaborate calculation program, exploiting the different equations found by our model in the previous chapters, as well as to compare them with the results obtained by the perfect gas model and the high temperature model.

A- Application in Open Systems: Isentropic flow in supersonic MLN nozzle

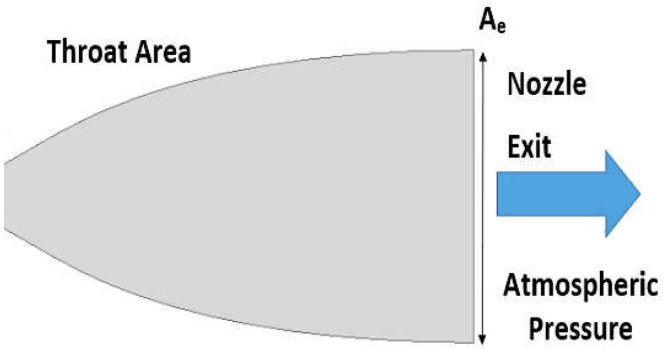

Figure 2. Sketch of Minimum length nozzle divergent

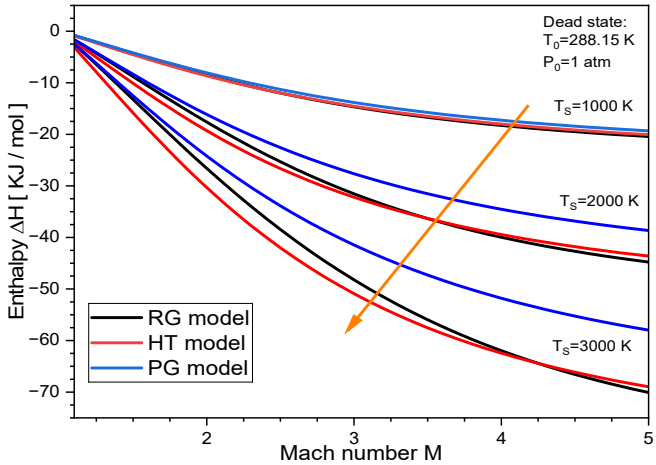

Figure 3. Variation of enthalpy as a function of Mach number

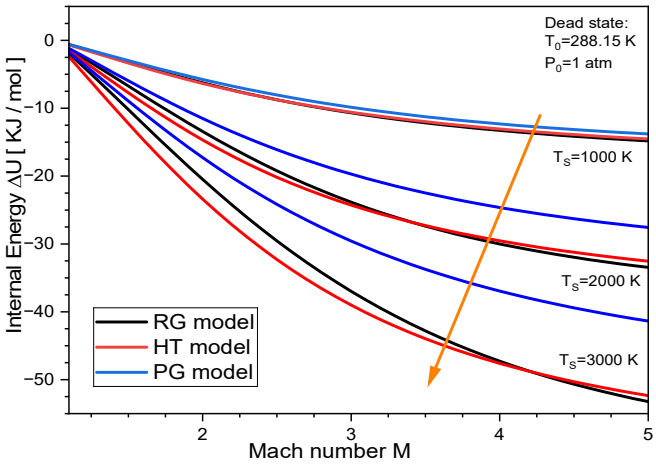

Figure 4. Variation of internal energy as a function of Mach number

This graph compares the specific internal energy ΔU of real gas RG, high temperature HT, and perfect gas PG models for compressible flow at three stagnation temperatures T_0=1000, 2000, and 3000 K.At low Mach numbers near unity, the curves almost overlap for all models and temperatures, demonstrating that internal energy predictions are rather insensitive to real gas and high temperature effects in the weakly compressible zone. As Mach number and stagnation temperature increase, however, systematic differences arise: the PG model predicts the largest decrease in ΔU, whereas RG and HT models show a smaller reduction, reflecting the influence of temperature dependent specific heats and excitation of additional molecular degrees of freedom that moderate the drop in internal energy. At high Mach numbers M>4 and T_0=3000 K, these discrepancies become pronounced, underscoring that use of a perfect gas model in high speed, high temperature nozzle or turbine flows can significantly misrepresent the internal energy field and thus affect subsequent calculations of exergy, entropy generation, and thermal loading.

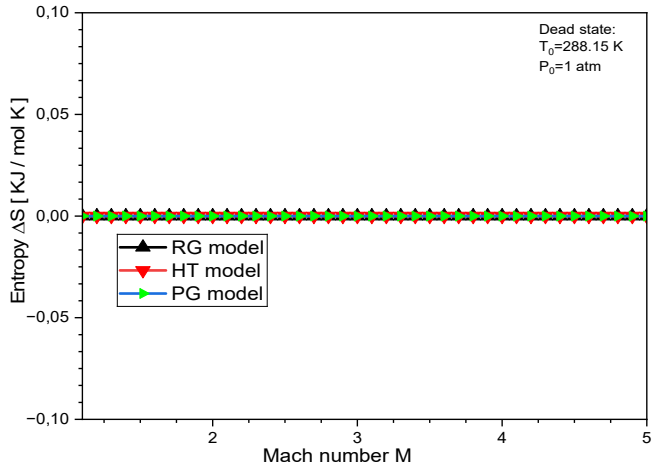

Figure 5. Variation of entropy as a function of Mach number

This Figure 5 illustrates the variation of entropy change Δs with Mach number for compressible flow, comparing realgas RG, high temperature HT, and perfect gas PG models, and shows that all curves collapse onto a single line with Δs≈0 over the entire Mach range. The near-zero entropy change confirms that the nozzle flow is effectively isentropic, meaning that despite large variations in velocity, pressure, and temperature, the combined effects of compressibility and thermodynamic property variations do not introduce significant irreversibilities in the modeled cases. The absence of discernible differences between RG, HT, and PG predictions emphasizes that, for an idealized adiabatic and frictionless expansion, realgas and high temperature corrections have negligible influence on entropy, even though they substantially affect enthalpy and internalenergy distributions, thereby justifying the use of any of the three models for purely entropy-based assessments of such flows.

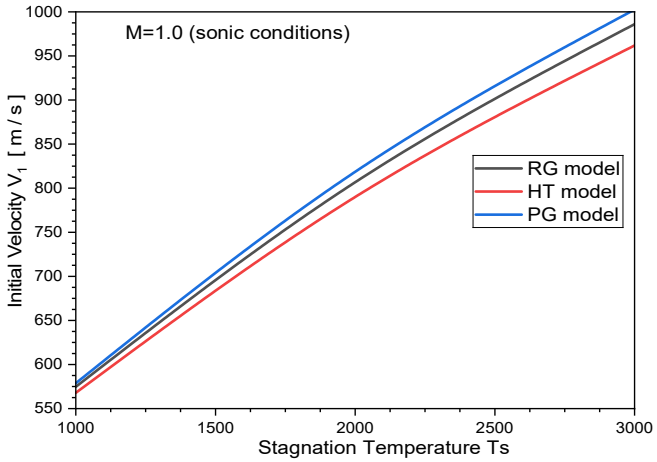

Figure 6. Variation of inlet velocity as a function of stagnation temperature

The Figure 6 illustrates how the initial flow velocity at sonic conditions increases monotonically with stagnation temperature, and how the prediction depends on whether a perfect gas PG, high temperature HT, or real gas RG model is used. For a given Mach number M=1, the PG model assumes constant specific heats and therefore gives the largest velocities at high stagnation temperatures because the stagnation enthalpy grows linearly with temperature and no additional internal modes or realgas effects absorb energy. The HT model partially accounts for temperature-dependent specific heats, which lowers the effective speed of sound and hence the calculated flow velocity, producing the lowest curve over most of the temperature range. The RG model further incorporates non-ideal behavior at high pressures and temperatures, such as changes in the equation of state and the caloric imperfections, leading to intermediate velocities between PG and HT or, in some ranges, closer agreement with experimental data for high enthalpy nozzles and rocket flows. Physically, the Figure highlights that as stagnation temperature rises (e.g., from 1000 K to 3000 K) the available stagnation enthalpy increases and thus the sonic flow issues with higher velocity, but it also shows that neglecting caloric and realgas effects can over predict this velocity by several percent in high temperature propulsion applications like plug or dualexpansion nozzles.

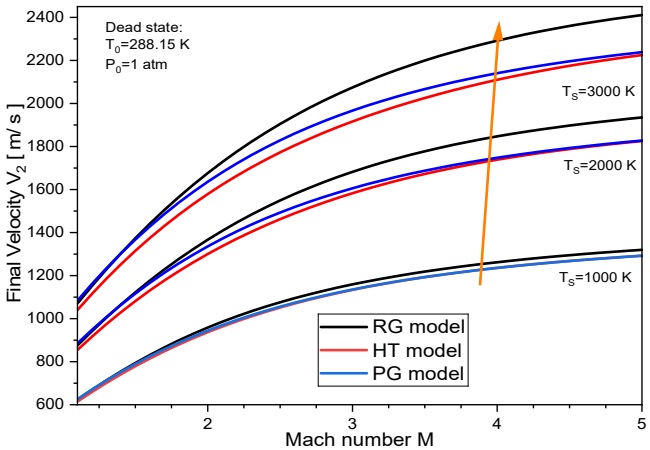

Figure 7. Variation of outlet velocity as a function of Mach number

The Figure 7 demonstrates that the final flow velocity increases with both Mach number and stagnation temperature, and that the choice of perfect gas PG, high temperature HT, or real gas RG model significantly affects the predicted values. For example, at Ts=1000 K and M=5, all three models converge to a final velocity of about 1150–1200 m/s, consistent with classical compressible flow estimates using a calorically perfect gas with $\gamma \approx 1.4$. In contrast, at Ts=3000 K and the same Mach number, the PG model predicts a velocity close to 2350 m/s, whereas the HT model yields roughly 2200 m/s and the RG model about 2400 m/s, because temperature-dependent specific heats

and non-ideal equation of state effects reduce or enhance the portion of stagnation enthalpy that can be converted into directed kinetic energy.Around M=3, the spread among models is smaller for Ts=2000 K, the PG curve lies near 1700 m/s, the HT curve near 1600 m/s, and the RG curve slightly above 1750 m/s highlighting that real gas corrections become more pronounced as both Mach number and stagnation temperature depart from the low-speed, low-enthalpy regime associated with a dead state of T_0=288.15 K and P_0=1 atm.

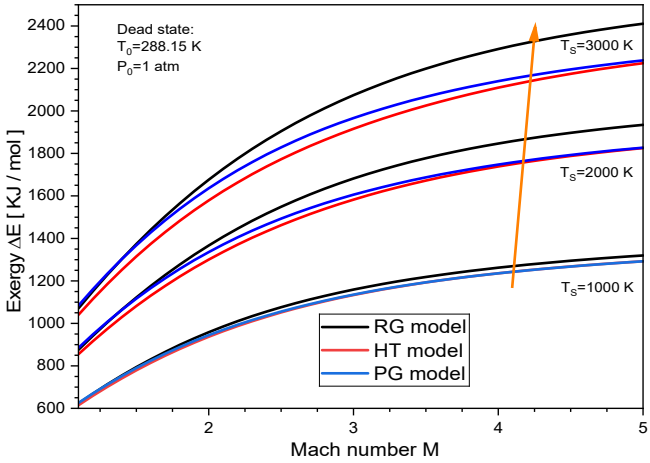

Figure 8. Variation of exergy as a function of Mach number

The Figure 8 presents the variation of flow exergy ΔE with Mach number for three thermodynamic models perfect gas PG, high temperature HT, and real gas RG at stagnation temperatures of 1000, 2000, and 3000 K, evaluated with respect to a dead state of T_0=288.15 K and P_0=1 atm. At the lowest stagnation temperature Ts=1000 K and M=5, all models give similar exergy levels around 1200–1300 kJ/mol, reflecting the near-ideal behavior of the gas when temperature is only moderately above the dead state value and non-ideal effects are weak. In contrast, for Ts=3000 K and M=5 the RG curve approaches roughly 2400 kJ/mol, while the PG and HT models predict about 2300 kJ/mol and 2200 kJ/mol respectively, because temperature-dependent specific heats and realgas equations of state alter the recoverable work from the same stagnation enthalpy rise. Around M=3 and Ts=2000 K, the PG and HT models cluster near 1600–1700 kJ/mol, whereas the RG model lies closer to 1800 kJ/mol, illustrating that realgas corrections become increasingly important as both Mach number and stagnation temperature increase, thereby influencing secondlawbased performance metrics such as nozzle efficiency and flow engine work potential.

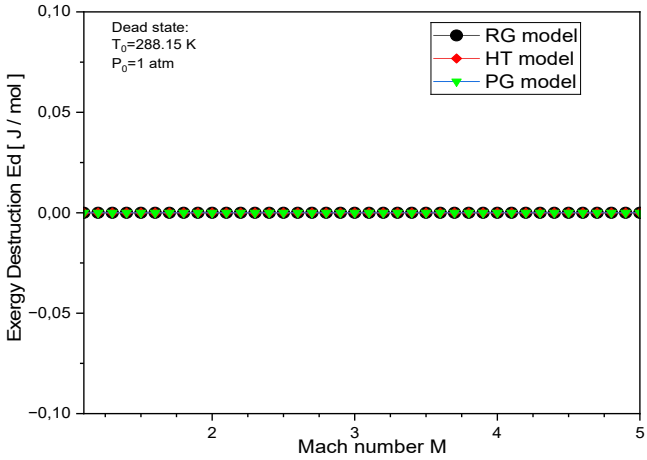

Figure 9. Variation of exergy destruction as a function of Mach number

The Figure 9 shows that the exergy destruction Ed is basically minimal throughout the measur ed Mach number range, with values ranging about 0.00 J/mol between M=1.0 and M=5.0 for all thr ee thermodynamic models RG, HT, and PG. The plotted data suggest that even at higher

supersonic conditions, for example at M=3.0 or M=4.5, the exergy destruction does not exceed roughly 1×10^{-3} J/mol, indicating an almost reversible behavior under the specified dead state of T_0=288.15 K and P_0=1 atm. The close overlap of the RG, HT, and PG curves demonstrates that, within this flow regime and reference environment, the choice of thermodynamic model exerts only a marginal influence on the predicted exergy losses, so that all three approaches effectively collapse onto a single curve with Ed≈0.00 J/mol for practical purposes.

B- Application in closed Systems:

1- Isochoric process: Air Tank

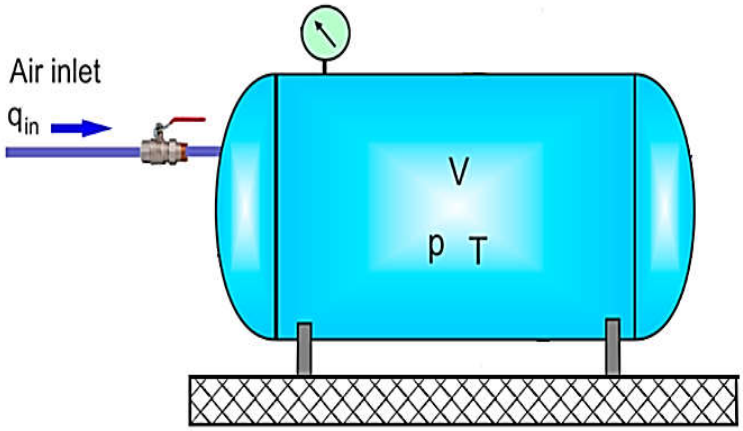

Figure 10. Sketch of air tank

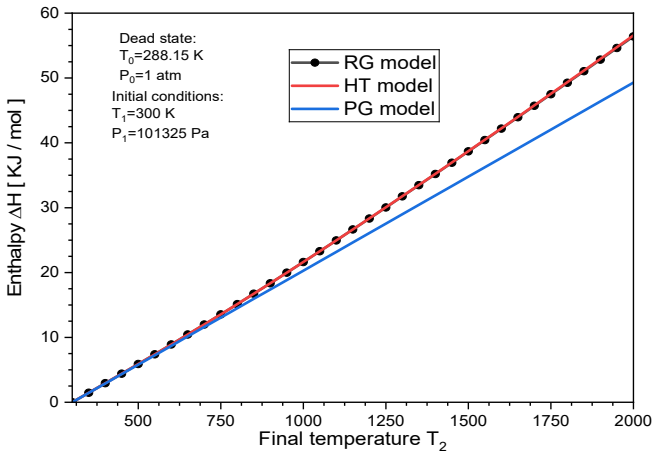

Figure 11. The enthalpy change versus the final temperature

The Figure 11 shows that the enthalpy change ΔH increases almost linearly with the final temperature T_2 for all three thermodynamic models, but with noticeable differences at high temperature. For moderate heating, say from the initial condition T_2=300 K to 1000 K, the RG and HT models predict nearly identical enthalpy increments of roughly 30 kJ/mol, whereas the PG model under predicts slightly, giving about 27 kJ/mol. At a much higher temperature, such as T_2=1800 K, the divergence becomes more pronounced: the RG and HT curves reach values close to 55 kJ/mol, while the PG model remains near 48 kJ/mol, highlighting the growing importance of real gas and high temperature effects as the temperature departs substantially from the ambient dead state (T_0=288.15 K,P_0=1atm).

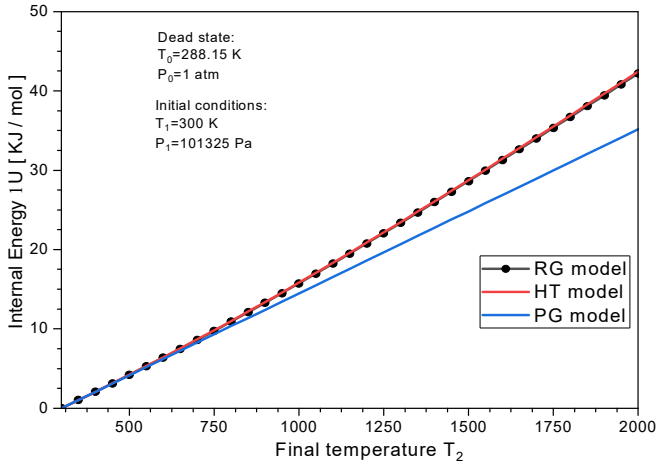

Figure 12. The internal energy change versus the final temperature

The Figure 12 compares the variation of molar internal energy ΔU with the final temperature T_2 for three thermodynamic gas models RG, HT, and PG over roughly 300–2000 K, showing that the real gas RG and high temperature HT models nearly coincide while the perfect gas PG model underpredictsΔU at high temperatures For example, at a moderate final temperature of about 800 K, the RG and HT curves deliver ΔU≈15 kJ/mol, whereas the PG model yields closer to 12 kJ/mol, demonstrating that assuming constant specific heats leads to a smaller energy rise for the same temperature change. At T_2≈1500 K, the discrepancy grows more pronounced, with RG and HT predicting around 32–34 kJ/mol compared with roughly 27–28 kJ/mol for the PG line, which is consistent with the strong temperature dependence of cv in combustion products. Near the upper end of the range, around 2000 K, the RG model approaches ΔU≈45 kJ/mol while the PG model remains nearer 36– 38 kJ/mol, indicating that real gas effects and variable specific heats become essential for accurately capturing internal energy changes in high temperature gas turbine or rocket chamber conditions.

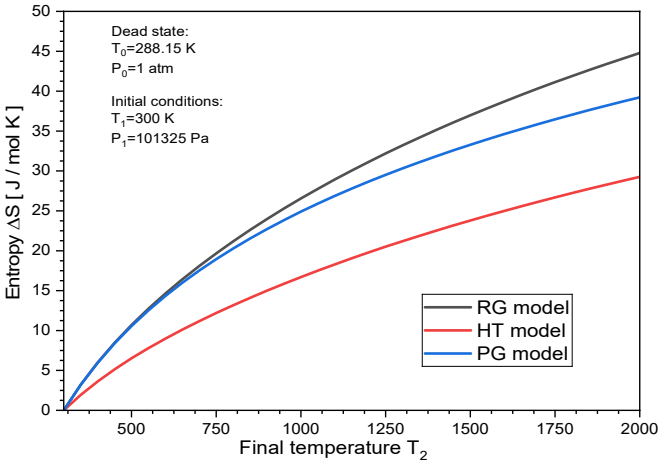

Figure 13. The entropy change versus the final temperature

The Figure 13 illustrates the dependence of the entropy change Δs on the final temperature T_2thermodynamic gases when modeled as a real gas RG, a high temperature gas HT, and a perfect gas PG, revealing systematic differences that grow with temperature. At a moderate temperature of T_2≈800 K, the RG curve predicts an increase in entropy of around 12 J/mol·K. The HT and PG models, on the other hand, predict smaller increases of about 9 and 10 J/molK, respectively. This shows that ignoring real gas effects tends to make entropy generation at this state seem lower than it really is. Moving to T_2≈1500 K, Δs rises to nearly 30 J/molK for the RG model, while the PG and HT curves lie lower, near 26 and 22 J/molK, highlighting that the simplified models increasingly underestimate the extent of molecular disorder introduced by heating. Near the upper limit, at T_2≈2000 K, the divergence becomes more pronounced, with the RG model reaching about 46 J/molK compared with only around 40 J/mol K for the PG model and 33 J/molK for the

HT model, underscoring that accurate high temperature cycle or exergy analyses must account for both temperature-dependent properties and gaseous imperfections behavior to avoid significant errors in entropy and, by extension, irreversibility predictions.

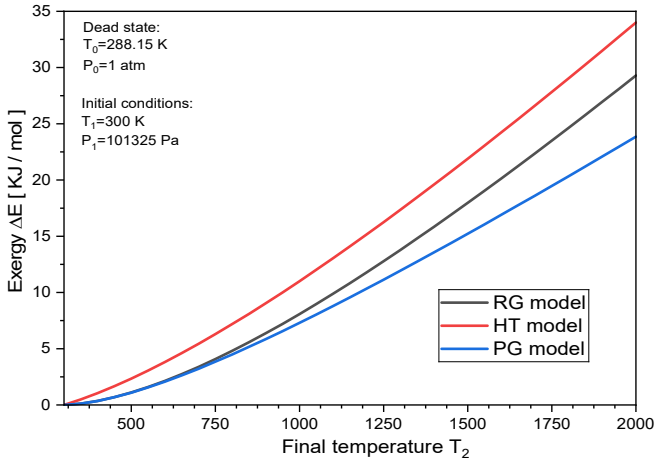

Figure 14. The exergy change versus the final temperature

The exergy–temperature graph in Figure 14 shows how the maximum useful work ΔE of the thermodynamic gas models increases nonlinearly with the final temperature T_2 and how sensitive this prediction is to the underlying thermodynamic model. At a moderate temperature of about $T_2 \approx$ 800 K, the real gas RG and perfect gas PG models predict relatively similar exergy values, on the order of 6–7 kJ/mol, while the high temperature HT model already yields a slightly larger value of roughly 8 kJ/mol, reflecting the stronger influence of variable specific heats on available work as temperature rises. Around $T_2 \approx$1500 K, the HT curve clearly separates from the others, reaching nearly 20 kJ/mol compared with about 16–17 kJ/mol for the RG model and only 14–15 kJ/mol for the PG approximation, which would substantially underpredict the work potential of high temperature systems in gas-turbine or combined-cycle analyses for exemple. Near the upper limit, at $T_2 \approx$2000 K, the discrepancy becomes quite pronounced, the HT model indicates an exergy of roughly 34–35 kJ/mol, whereas the RG and PG models give about 28–30 kJ/mol and 24–26 kJ/mol, respectively, emphasizing that simplified assumptions about ideality and constant properties can lead to errors of 25–30% in estimating the theoretical work output of advanced high temperature energy conversion systems.

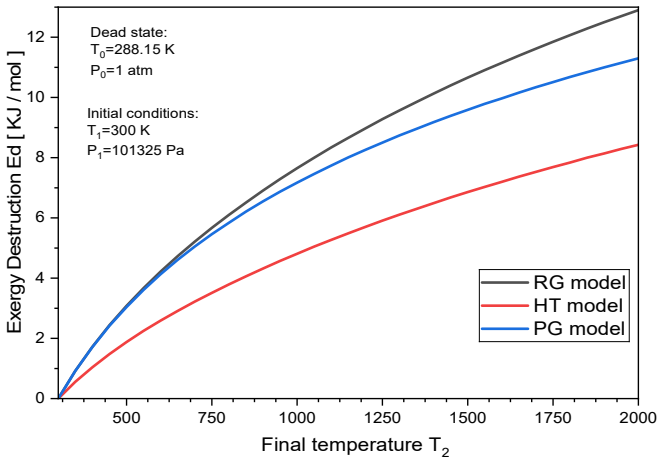

Figure 15. The exergy distruction versus the final temperature

The Figure 15 compares the variation of molar internal energy ΔU with the final temperature T_2 for three thermodynamics gas models RG, HT, and PG over roughly 300–2000 K, showing that the real gas RG and high temperature HT models nearly coincide while the perfect gas PG model under predicts ΔU at high temperatures. For instance, the RG and HT curves yield $\Delta U \approx$15 kJ/mol at a modest ultimate temperature of roughly 800 K, whereas the PG model yields

closer to 12 kJ/mol. This shows that assuming constant specific heats results in a reduced energy rise for the same temperature change.At $T_2 \approx 1500$ K, the discrepancy grows more pronounced, with RG and HT predicting around 32–34 kJ/mol compared with roughly 27–28 kJ/mol for the PG line, which is consistent with the strong temperature dependence of cv in combustion products. Near the upper end of the range, around 2000 K, the RG model approaches $\Delta U \approx 45$ kJ/mol while the PG model remains nearer 36–38 kJ/mol, indicating that real gas effects and variable specific heats become essential for accurately capturing internal energy changes in high temperature conditions.

2- Isobaric process: Piston-cylinder

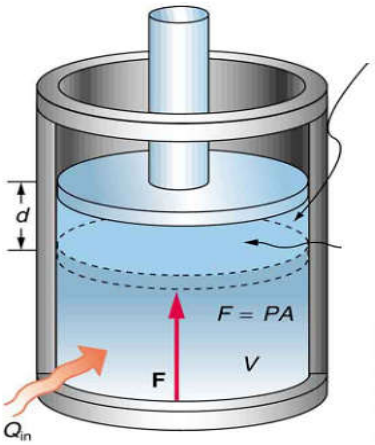

Figure 16. Scatch of piston-cylinder

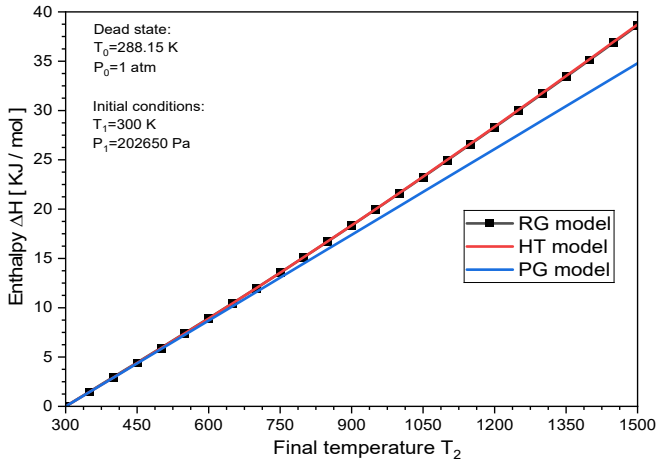

Figure 17. The enthalpy variation versus the final temperature

The Figure 17 compares the variation of molar enthalpy change ΔH with final temperature T_2 for three thermodynamic models, a real gas RG model, a high temperature HT model, and a perfect gas PG model, all starting from an initial state of T_1=300 K and $P_1 \approx 2.0 \times 10^5$ Pa. At low temperatures, around T_2=400 K, all three models predict nearly the same enthalpy change, on the order of 2–3 kJ/mol, reflecting the weak temperature dependence of heat capacity and minimal non-ideal effects in this range. As the temperature increases to about T_2=900 K, the PG line remains linear with a slope corresponding to an almost constant Cp, giving, for example, $\Delta H \approx 20$ kJ/mol, whereas the RG and HT curves lie slightly above, indicating an effective heat capacity that grows with temperature so that ΔH reaches roughly 22–23 kJ/mol at the same T_2.Near the upper end of the plotted range, around T_2=1500 K, the discrepancy becomes more pronounced, the PG model may predict an enthalpy change of about 32 kJ/mol, while the RG and HT models approach $\Delta H \approx 38$–39 kJ/mol, underlining how gaseous imperfections behavior and temperature-dependent substantially affect energy accounting at very high temperatures, a point that is particularly relevant when estimating exergy relative to the dead state at $T_0 \approx 298$ K and P_0=1 atm.

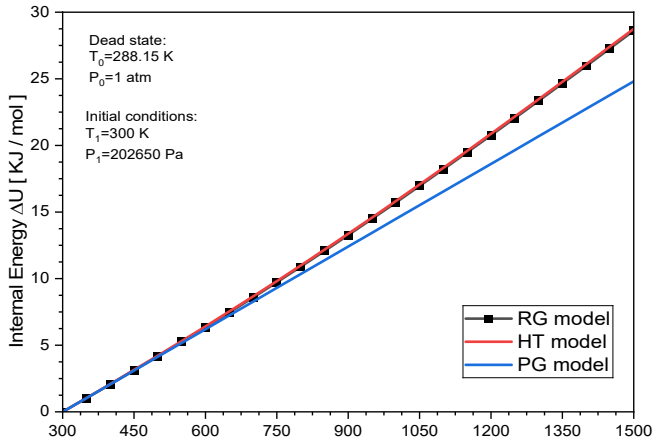

Figure 18. The internal energy variation versus the final temperature

The Figure 18 depicts how the molar internal energy change ΔU varies with the final temperature T_2 for a real gas RG model, a high temperature HT model, and a perfect gas PG model, starting from T_1=300 K and $P_1 \approx 2.0\times10^5$ Pa. At modest temperatures, for example around T_2=400 K, the three curves nearly coincide, predicting ΔU≈1–2 kJ/mol, which indicates that non-ideal effects and the temperature dependence of Cv are still weak in this regime. As the temperature rises to T_2=900 K, the PG model maintains an almost perfectly linear trend with ΔU of roughly 15 kJ/mol, while the RG and HT predictions climb slightly higher to about 16–17 kJ/mol, suggesting an effective increase in Cv associated with molecular excitation at elevated temperatures. At the upper end of the domain near T_2=1500 K, the difference becomes more evident, the PG model yields ΔU≈24–25 kJ/mol, whereas the RG and HT models give values closer to 28–29 kJ/mol, emphasizing that accurate high temperature internal energy calculations require non-ideal and temperature-dependent property models rather than the simplified perfect gas assumption when evaluating processes referenced to a dead state at T_0≈298 K and P_0=1 atm.

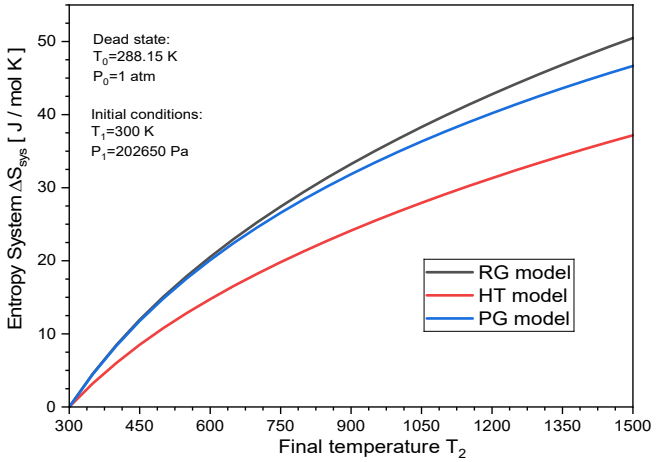

Figure 19. The system entropy variation versus the final temperature

The Figure 19 illustrates the dependence of the system entropy change ΔS sys on the final temperature T_2 for real gas RG, high temperature HT, and perfect gas PG models, starting from T_1=300 K and $P_1 \approx 2.0\times10^5$ Pa. At moderate heating to about T_2=500 K, the PG curve already predicts ΔS sys of roughly 8 – 9 J/molK, while the RG model is slightly higher near 10 J/mol·K and the HT model gives a smaller increase, about 6 – 7 J/molK, emphasizing the sensitivity of entropy to the adopted temperature-dependent heat capacity correlations. As the temperature reaches T_2=900 K, the PG and RG curves show larger entropy rises of around 20 –22 J/molK, whereas the HT model still lags at approximately 15– 16 J/molK, reflecting its different treatment of molecular excitations and non-ideal interactions at high temperature. Near the upper bound of the plot, around T_2=1500 K, the RG model predicts the largest entropy change, approaching 35– 36 J/molK, followed closely by the PG model at roughly 33– 34 J/molK, while the HT model remains significantly lower at about 27– 28 J/molK; this divergence highlights that entropy, more than

enthalpy or internal energy, can be strongly affected by the detailed form of Cp(T) and by real gas effects, which is crucial when computing exergy relative to the dead state at T_0≈298 K and P_0=1 atm.

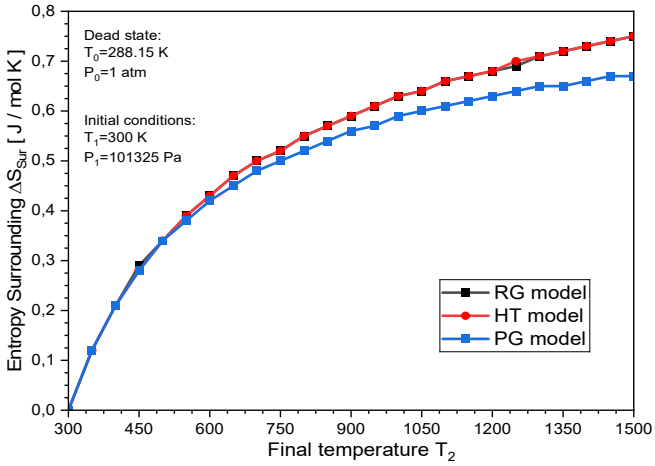

Figure 20. The surrounding enthalpy variation versus the final temperature

The Figure 20 shows how the entropy change of the surroundings ΔSsur varies with the final temperature T_2 for real gas RG, high temperature HT, and perfect gas PG models, when the system initially is at T_1=300 K and P_1=2.0×10^5 atm. At moderate heating from 300 K to about T_2=500 K, all three models predict a relatively small entropy increase of the surroundings, on the order of 0.25– 0.30 J/molK, because the heat exchanged with the environment at the dead state temperature T_0≈298 K remains limited in this range. As the final temperature rises to T_2=900 K, the PG curve gives ΔSsur≈ 0.50 J/molK, while the RG and HT models show slightly higher values around 0.55– 0.60 J/molK, reflecting the larger heat transfer implied by their higher predicted enthalpy changes. Near T_2=1500 K, the influence of the property model becomes more pronounced, the PG model yields ΔSsur ≈0.65–0.70 J/molK, whereas the HT and RG models approach roughly 0.75–0.80 J/molK, indicating that non-ideal and temperature dependent heat capacity effects modestly increase the entropy exported to the surroundings during strong heating, which is a key contribution to the overall exergy destruction in high temperature processes referenced to the dead state T_0 and P_0.

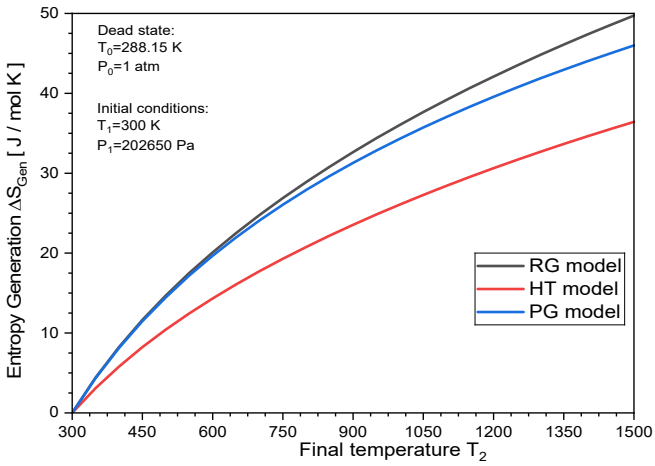

Figure 21. The generation enthalpy variation versus the final temperature

The Figure 21 presents the entropy generation ΔS gen as a function of the final temperature T_2 for real-gas RG, high temperature HT, and perfect gas PG models, starting from T_1 =300 K and P_1≈2.0×10^5 Pa, with the environment at the dead state T_0=288.15 K and P_0=1 atm. For modest heating to T_2=500 K, all three models predict relatively small entropy generation, on the order of 6–7 J/molK, because the process is only mildly irreversible in this range. As the final temperature increases to around T_2=900 K, the PG curve gives ΔS gen≈23–24 J/molK, the RG

model lies slightly higher near 25–26 J/molK, while the HT model is significantly lower at about 18–19 J/molK, showing that different treatments of temperaturedependent heat capacities and realgas effects can alter the predicted irreversibility by nearly 30%.At the upper end of the range, for T_2=1500 K, this divergence becomes even more pronounced: the PG model predicts ΔS gen of roughly 40–42 J/molK, the RG model gives the highest value close to 48–50 J/molK, whereas the HT model yields only about 33–35 J/molK, implying that accurate modeling of high temperature processes is essential for realistic estimation of entropy generation and thus of exergy destruction in engineering systems.

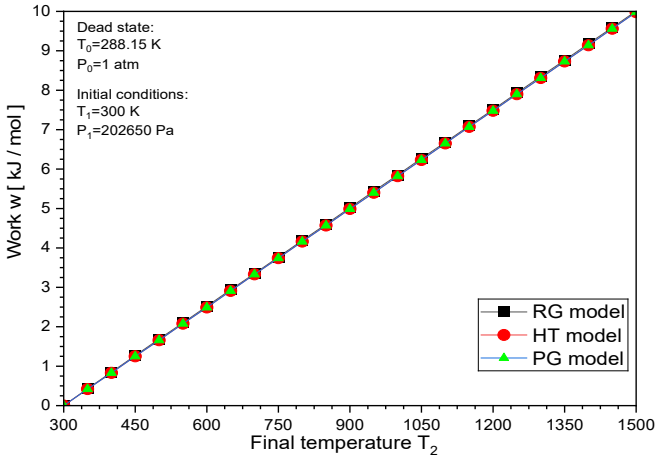

Figure 22. The work versus the final temperature

The Figure 22 displays the work W delivered by the system as a function of the final temperature T_2 for real gas RG, high temperature HT, and perfect gas PG property models, starting from T_1=300 K and $P_1 \approx 2.0\times10^5$ Pa with the environment at the dead state T_0=288.15 K and P_0=1 atm. The three curves practically coincide over the entire range, indicating that the evaluated work is almost insensitive to the particular thermodynamic model used under these conditions. For moderate heating to T_2 =600 K, all models predict a work output of about 3.5–3.6 kJ/mol, while at T_2=900 K the work increases linearly to nearly 5.5–5.6 kJ/mol, showing that the process behaves with an almost constant effective pressure–volume relationship. At the upper end of the range, for T_2=1500 K, the predicted work rises to roughly 9.5–9.6 kJ/mol for all three models, confirming that, despite earlier differences observed in enthalpy, internal energy, and entropy, the net macroscopic work associated with the considered path is governed primarily by the imposed boundary conditions rather than by subtle differences in realgas versus perfectgas behavior.

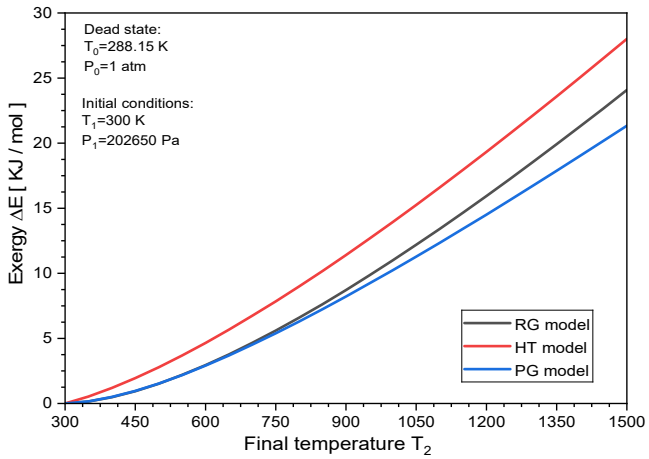

Figure 23. The exergy variation versus the final temperature

The Figure 23 describes the exergy change ΔE of the system as a function of the final temperature T_2 for real gas RG, high temperature HT, and perfect gas PG models, with the dead state specified as T_0=288.15 K and P_0=1 atm and the initial state at T_1=300 K and $P_1 \approx 2.0\times10^5$ Pa. For moderate heating to T_2=600 K, all three models still predict relatively small exergy increases

of roughly 3–4 kJ/mol, but a clear separation already appears, the HT model yields the largest exergy about 4 kJ/mol, followed by the RG prediction around 3.5 kJ/mol, while the PG model gives only about 3 kJ/mol. As the temperature is raised to T_2=1000 K, the curvature in all three curves becomes evident, with exergy values of approximately 10–11 kJ/mol for PG, 12–13 kJ/mol for RG, and nearly 15 kJ/mol for the HT model, illustrating that exergy grows faster than linearly with temperature because both available work from enthalpy and the entropy deficit relative to the environment increase.At the upper limit of the plot, T_2=1500 K, this trend is accentuated: the PG model gives $\Delta E \approx 18–19$ kJ/mol, the RG model predicts roughly 21–22 kJ/mol, and the HT model reaches about 26–27 kJ/mol, highlighting that high temperature correlations and gaseous imperfections effects can change the estimated available work by more than 40% compared with a simple perfectgas analysis, which is critical when sizing high temperature power or propulsion systems.

The Figure 24 depicts the exergy destruction Ed as a function of the final temperature T_2 for realgas (RG), high temperature HT, and perfectgas PG models, for a system initially at T_1=300 K and $P_1 \approx 2.0\times10^5$ Pa and exchanging heat with an environment at the dead state T_0=288.15 K and P_0=1 atm. At relatively low final temperatures, for example T_2=500 K, the exergy destruction is still modest, with all models predicting approximately 3–4 J/mol, and the HT curve already lying slightly below the PG and RG curves, indicating a somewhat less irreversible process when high temperature heatcapacity effects are accounted for. As the final temperature increases to around T_2=900 K, the PG and RG descriptions converge to Ed ≈8–9 J/mol, whereas the HT model gives only about 6–7 J/mol, suggesting that simplified property models may overestimate the entropy generation and thus the destroyed available work in high temperature applications. Near T_2=1500 K, the divergence between the models becomes more pronounced: the RG curve reaches exergy destruction values close to 13–14 J/mol, the PG model follows slightly lower at roughly 12–13 J/mol, while the HT model remains significantly smaller at about 10–11 J/mol, highlighting that the choice of thermodynamic model can change the predicted irreversibility by nearly 30%, which is critical when performing detailed exergy accounting and optimization of high temperature energy conversion systems.

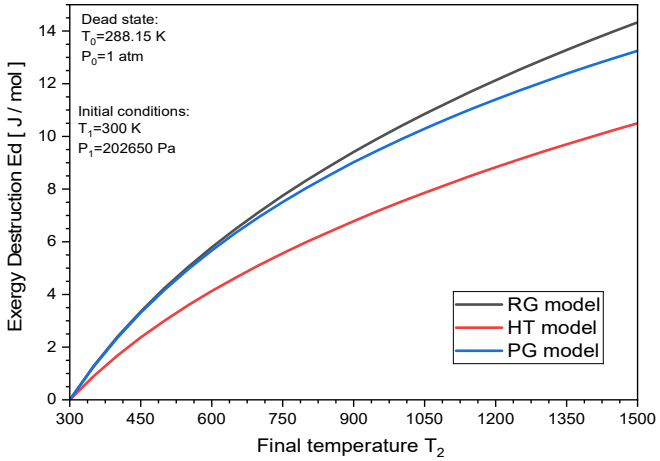

Figure 24. The exergy distruction versus the final temperature

The Figure 24 depicts the exergy destruction Ed as a function of the final temperature T_2 for realgas (RG), high temperature HT, and perfectgas PG models, for a system initially at T_1=300 K and $P_1 \approx 2.0\times10^5$ Pa and exchanging heat with an environment at the dead state T_0=288.15 K and P_0=1 atm. At relatively low final temperatures, for example T_2=500 K, the exergy destruction is still modest, with all models predicting approximately 3–4 J/mol, and the HT curve already lying slightly below the PG and RG curves, indicating a somewhat less irreversible process when high temperature heatcapacity effects are accounted for. As the final temperature increases to around T_2=900 K, the PG and RG descriptions converge to Ed ≈8–9 J/mol, whereas the HT model gives only about 6–7 J/mol, suggesting that simplified property models may overestimate the entropy generation and thus the destroyed available work in high temperature applications. Near T_2=1500 K, the divergence between the models becomes more pronounced: the RG curve reaches exergy destruction values close to 13–14 J/mol, the PG model follows slightly lower at roughly 12–13 J/mol, while the HT model remains significantly smaller at about 10–11 J/mol, highlighting that

the choice of thermodynamic model can change the predicted irreversibility by nearly 30%, which is critical when performing detailed exergy accounting and optimization of high temperature energy conversion systems.

5. Conclusion

This work consolidates and extends earlier exergybased investigations by demonstrating that exergy analysis is a decisive tool for revealing the real thermodynamic performance and hidden inefficiencies of energy systems, and, building on all previous exergy investigations, it introduces a rigorous exergy formulation explicitly derived for real gases, thereby removing the idealizing assumptions embedded in conventional HT and GPbased approaches that rely on perfect gas behavior.Through a systematic decomposition of exergy streams and destruction mechanisms, the study identifies the components and operating conditions that dominate irreversibility, thereby indicating where design and operational improvements will yield the highest thermodynamic and economic benefits, while the consistent incorporation of real-gas thermodynamic properties over the full range of operating pressures, temperatures and compositions enables the new model to capture gaseous imperfections effects that HT and GP formulations systematically neglect, leading to more accurate prediction of exergy, exergy destruction and exergy efficiencies in highly compressed and strongly non-isothermal flows.The results confirm that firstlaw metrics alone systematically underestimate the improvement potential, whereas exergybased indicators provide a rational basis for prioritizing retrofits, guiding advanced control strategies and integrating emerging technologies; at the same time, comparative calculations demonstrate that, in operating domains where the perfectgas hypothesis is only marginally valid, HT and GP may significantly underestimate irreversibilities and mis-rank the most critical components, whereas the proposed real-gas exergy form preserves the correct ordering of losses and the correct magnitude of improvement potential. As a result, the present contribution offers a coherent exergy framework that can be readily transferred to other conFigureurations, scales and sectorsfrom conventional thermal power plants to integrated lowcarbon systemsand provides a more reliable thermodynamic basis for optimization, control and design of advanced energy and process systems in which non-ideal gas behavior plays a central role, while future research should deepen this approach by coupling advanced and dynamic exergy analyses with lifecycle and economic assessments, enabling decisionmakers to evaluate design choices in terms of resource quality, environmental impact and longterm sustainability in a unified manner.

REFERENCES

[1] *C. Borgnakke and R. E. Sonntag, "Fundamentals of Thermodynamics", Wiley, Hoboken,* ***(2013).***

[2] *J. E. Ahern and D H Johnson, "The Exergy Method of Energy Systems Analysis», Journal of Solar Energy Engineering., vol. 104, no. 1,* ***(1982)****, pp. 1-56. https://doi.org/10.1115/1.3266277*

[3] *I. Dincer and M. A. Rosen, "Exergy: Energy, Environment and Sustainable Development ", Elsevier, oxford,* ***(2020).***

[4] *L. Borel, D. Favrat, D. L. Nguyen and M. Batato, "Thermodynamics and Energy Systems Analysis", EPFL Press, Lausanne,* ***(2010).***

[5] *E. Michaelides, "Exergy Analysis for Energy Conversion Systems", University Press, Cambridge,* ***(2021).***

[6] *T. J. Kotas, "the Exergy Method of Thermal Plant Analysis", Butterworths, Boston,* ***(1985).***

[7] *M. J. Moran and H. J. Shapiro, "Fundamentals of Engineering Thermodynamics", John Wiley & Sons Inc, Chichester,* ***(2006).***

[8] *C. A. Frangopoulos, "Exergy, Energy System Analysis, and Optimization", EOLSS Publishers Company Limited, UK,* ***(2009).***

[9] *K. Annamalai and K. P. Ishwar, "Advanced Thermodynamics Engineering", CRC Press LLC, Florida,* ***(2002).***

[10] *M. K. Irving and R. M. Rosenberg, "Chemical Thermodynamics: Basic Concepts and Methods", John Wiley & Sons Inc, New Jersey,* ***(2008).***

[11] *S. Lu, X. Yang, N. Yu, S. Bu, W. Li, J. Liu, W. Dai and X. Wang, "Energy, exergy, economic, and environmental analysis and comprehensive competence assessment of a DS-DPORC system utilizing industrial residual heat: an advanced exergy analysis approach", Thermal Science and Engineering Progress., vol. 68, no. , **(2025)**, pp. 104265-104282 https://doi.org/10.1016/j.tsep.2025.104265.*

[12] *F. N. Izzah, B. F. T. Kiono and K. Rozi, "Energy and exergy analysis of the XYZ ultra-supercritical steam power plant ", Green technology & Innovation GTI., vol. 1, no. 1, **(2025)**, pp.1-14 https://doi.org/10.36922/gti.8099*

[13] *M. Fallah, Z. Mohammadi, S. Allahyari, S. H. Rahimi, M . FATHI, Z. Hoseini Tabar and S. M. S. Mahmoudi, "Comprehensive review of methodologies and case studies in advanced exergy, exergo-economic, and exergo-environmental analyses ",Energy., vol. 334, no. 1 , **(2025)**, pp. 137606- 137629 https://doi.org/10.1016/j.energy.2025.137606.*

[14] *H. M. Brilliant, "Analysis of Scramjet Engines Using Exergy Methods",31st AlAA Joint Propulsion Conference and Exhibit, San Diego, California, USA, (1995) July 10 - 12 , Abstracts p- 2767 , AIAA 95-2724*

[15] *R. K. Rajput, "Engineering Thermodynamics", Laxmi Publications, New Delhi, INDIA,* ***(2007).***

[16] *T. Zebbiche, " Tuyères Supersoniques à Haute Température: Effet de la température génératrice sur la conception et le dimensionnement des diverses formes des tuyères supersoniques ", EditionsUniversitaires Européennes, Sarrebruck,* ***(2010).***

[17] *Y. Cengel, M. Boles and M. Kanoglu, "Thermodynamics: An Engineering Approach", McGraw-Hill, NewYork,* ***(2018).***

[18] *T. Yahiaoui, T. Zebbiche, A. Allali and M. Boun-jad, "Gas effect for oblique and conical shock waves at high temperature", Mathematical Modelling of Natural Phenomena., vol. 15 , no. 73, **(2020)**, pp.1-26 https://doi.org/10.1051/mmnp/2020036*

[19] *T. Zebbiche and Z. Youbi, "Effect of stagnation temperature on the supersonic flow parameters with application for air in nozzles", The Aeronautical Journal., vol. 111, no. 1115, **(2007)**, pp.31-40 https://doi.org/10.1017/S0001924000001731*

[20] *T. Zebbiche and Z. Youbi, "Supersonic Two-Dimensional Minimum Length Nozzle Design at High Temperature. Application for Air",42nd AIAA/ASME/SAE joint propulsion conference & Exhibit, Sacramento, California, USA, (2006) July 09-12, Abstracts p - AIAA 2006-4599, https://doi.org/10.2514/6.2006-4599*

[21] *T. Zebbiche, "Stagnation Temperature Effect on the Prandtl Meyer Function",AIAA Journal., vol. 4, no. 54, **(2007)**, pp. 952- 953 https://doi.org/10.2514/1.24868*

[22] *T. Zebbiche and Z. Youbi, "Design of Two-Dimensional Supersonic Minimum Length Nozzle at Higth Temperature, Application for Air",German Aerospace Congress DGLR , Friendrichshafen, Germany, (2005) September 26 -29, Abstracts p - DGLR-2005-0256*

[23] *T. Zebbiche, "New Generalized Form of the Prandtl Meyer Function. Application for Air at High Temperature",25th AIAA Applied Aerodynamics*

Conference, San Francisco, USA, (2006) 25-28 June, Abstracts p - AIAA 2006-3674 , https://doi.org/10.2514/6.2006-3674

[24] *T. Zebbiche and Z. Youbi, " Supersonic Two-Dimensionnel Minimum Length Nozzle Design at High Temperature. Application for Air", Chinese Journal of Aeronautics., vol. 20, no. 1* ***(2007)****, pp. 29-39 https://doi.org/10.1016/S1000-9361(07)60004-1*

[25] *C. D. Donaldson, "Note on the Importance of ImperfectGas Effects and Variation of Heat Capacities on the IsentropicFlow of Gases", Advisory committee for aeronautics NACA, Document ID:19930085478, Report N° NACA-RM-L8J14, p 15Washington,* ***(1948).***

[26] *B. Ali Benyahia, S. Bensedira, M. Salhi and N. Bengherbia, "Vibrational Energy of Real Gas Molecules Impact on Calorimetric and Thermoelastic Coefficients", Indian Journal of Pure & Applied Physics., vol. 63, no. 12,* ***(2025)****, pp.1077-1087 DOI: 10.56042/ijpap.v63i12.14089*

[27] *M. Salhi , T. Zebbiche and A. Mehalem, "Stagnation pressure effect on the supersonic flow parameters with application for air in nozzles", The Aeronautical Journal., vol. 120, no. 1224,* ***(2016)****, pp. 313-354 https://doi.org/10.1017/aer.2015.13*

[28] *M. Salhi, "Gaseous imperfections effect on the supersonic flow parameters for air in nozzles",3rd International Conference and Exhibition on Mechanical & Aerospace Engineering, San Francisco, ,USA, (2015) October 05-07, , Abstracts pp. 122, http://dx.doi.org/10.4172/2168-9792.C1.011*

[29] *N. Bengherbia, M. Salhi and M. Roudane, "Normal shock waves through hypersonic flow in the presence of the vibrational energy and molecular dissociation effects", 1st National Conference on Materials Science and Applications ICMSA'23, khenchela ,Algeria, (2023) February 07 - 09, Abstracts pp. 163*

[30] *M. Salhi, T. Zebbiche and A. Mehalem, " Stagnation Pressure Effect on Prandtl Meyer Function for Air ", Proceedings of the Institute of Mechanical Engineering, Part G: Journal of Aerospace Engineering., vol. 231, no. 2,* ***(2017)****, pp. 326-337 https://doi.org/10.1177/0954410016636913*

[31] *M. Salhi and T. Zebbiche, "A New General Form of Prandtl Meyer Function, Application on Air" , 8thAIAA Theoretical Fluid Mechanics Conference, Denver, Colorado, USA, (2017) June 5-9, Abstracts p – 118*

[32] *N. Bengherbia, M. Salhi and M. Roudane, "Gas Effect with the presence of the thermal and calorific imperfections on the Prandtl Meyer function", Indian journal of physics., vol. 98, no. 7,* ***(2024)****, pp. 2461-2473 https://doi.org/10.1007/s12648-023-03004-3*

[33] *M. Roudane, M. Salhi and A. Boucherit, " A New Design Method for High Conditions Applied on Minimum length Nozzles ", Aerospace Research in Bulgaria., vol. 33, no.4,* ***(2021)*** *, pp. 167-183 http://journal.space.bas.bg/arhiv/n%2033/Articles/12_Roudane.pdf*

[34] *M. Salhi, "« Improvement of Supersonic Nozzles Performances by a New Design Method", Conference AIAA Aviation 2023 Forum, San Diego, California, USA, (2023) June 12–16, Abstracts p – AIAA 2023-3248, https://doi.org/10.2514/6.2023-3248*

[35] *M. Salhi, O. Ketfi and M. Roudane, "Numerical Investigation on New Models of the Internal Energy ΔU and the Work W", Romanian Journal of Physics., vol. 68, no. 609,* ***(2023)****, pp.1-18 https://rjp.nipne.ro/2023_68_3-4/RomJPhys.68.609.pdf*

[36] *M. Salhi, S. Bensedira and S. Bennoud, "Development and Investigation of a New General Model of Enthalpy", Journal of The Institution of Engineers (India): Series C., vol. 105, no. 5,* ***(2024)****, pp. 1047–1054 https://doi.org/10.1007/s40032-024-01115-2*

[37] *M. Salhi and M.Roudane, "Numerical Investigation of the Thermal Caloric Imperfections on entropy Enhancement across Normal Shock Waves", High Temperatures High pressures Journal vol. 48, no. 4,* ***(2019)****, pp. 1-24 DOI: 10.32908/hthp.v48.689*

[38] *M. Salhi, S. Bensedira, N. Bengherbia and M. Roudane, "Temperature-Pressure and Thermal- Caloric Imperfections Effects on Gibbs and Helmholtz Free Energies", Indian journal of physics., vol. 98, no. 14,* ***(2024)****, pp. 4849-4861 https://doi.org/10.1007/s12648-024-03237-w*

[39] *B. Domidovitch, and I. Maron "Elements de calcul numérique", MIR edition , Moscow,* ***(1979).***

[40] *D. J. Wilde, "Optimum Seeking Methods", Prentice-Hall press, Englewood Cliffs,* ***(1964).***

[41] *T. Zebbiche, M. Salhi and M. Boun-jad, "Numerical computational of supersonic flow around a pointed airfoil", Journal of computational methods in sciences and engineering., vol. 12, no. 3,* ***(2012)****, pp. 213-233 DOI: 10.3233/JCM-2012-0398*

[42] *T. J Ypma, " Historical Development of the Newton–Raphson Method ", SIAM Review., vol. 37, no. 4, (****1995)*** *, pp. 531-551 https://doi.org/10.1137/1037125*

[43] *A. Galántai. " The Theory of Newton's Method ", Journal of Computational and Applied Mathematics., vol. 124, no. 1–2,* ***(2000)****, pp. 25- 44 https://doi.org/10.1016/S0377-0427(00)00435-0*

[44] *L. Plaskota, "Automatic integration using asymptotically optimal adaptive Simpson quadrature", Numerische Mathematik., vol. 131, no. 1,* ***(2015)*** *, pp. 173-198 https://doi.org/10.1007/s00211-014-0684-3*

[45] *P. Houston and T. P. Wihler, "An Adaptive Variable Order Quadrature Strategy", (ICOSAHOM Conf. Proc. 533) (eds) M Bittencourt, N Dumont and J Hesthaven (Cham, Switzerland****:*** *Springer) p 533,* ***(2017)*** *, pp. 1-11 https://doi.org/10.48550/arXiv.1508.03516*